NASA/CR -97- 207773

Pergamon

Planet. Space Sci., Vol. 45, No. 10, pp. 1271–1277, 1997

0032–0633/97 $17.00+0.00

PII: S0032–0633(97)00075–5

REPRINT
IN-90-CR
OCIT
096459

Comet Shoemaker–Levy 9: an active comet

Terrence W. Rettig[1] **and Joseph M. Hahn**[2]

[1]Department of Physics, University of Notre Dame, Notre Dame, IN 46556, U.S.A.
[2]Lunar and Planetary Institute, 3600 Bay Area Boulevard, Houston, TX 77058-1113, U.S.A.

Received 30 September 1996; accepted 21 March 1997

Abstract. The important elements of the debate over the activity versus dormancy of comet Shoemaker–Levy 9 (S–L 9) are reviewed. It is argued that the circularity of the isophotes in the inner comae of S–L 9 as well as the spatial dependencies of the comae brightness profiles are indicators of sustained dust production by S–L 9. It is also shown that the westward tail orientations, which were formerly interpreted as a sign of the comet's dormancy, are *not* a good indicator of either activity or dormancy. Rather, the tail orientations simply place constraints on the dust production rate for grains smaller than $\approx 5\,\mu$m. All the available evidence points to S–L 9 as having been an active, dust-producing comet. Synthetic images of an active comet are fitted to Hubble Space Telescope images of the S–L 9 fragment K, and its grain size and outflow velocity distributions are extracted. These findings show that the appearance of the dust coma was dominated by large grains having radii between $\approx 30\,\mu$m and ≈ 3 mm, produced at a rate of $\dot{M} \approx 22$ kg s^{-1}, and ejected at outflow velocities of ≈ 0.5 m s^{-1}. Only upper limits on the production rates of smaller grains are obtained. The nucleus of fragment K was not observed directly but its size is restricted to lie within a rather narrow interval $0.4 \lesssim R_f \lesssim 1.2$ km.

Ever since the discovery of comet Shoemaker–Levy 9 (S–L 9) in the spring of 1993 there has been an ongoing debate regarding its activity (Sekanina *et al.*, 1994; Chernova *et al.*, 1996; Hahn *et al.*, 1996; Rettig *et al.*, 1996b; Sekanina, 1996a). This point is of no minor consequence, for in order to correctly understand the 1993–1994 observations of the S–L9 dust comae and tails it is necessary to know whether one was viewing recent and possibly ongoing dust emission, or perhaps more "ancient" dust emission that was triggered by the comet's tidal breakup in July 1992. Arguments for and against the comet's activity are described herein, and comparisons of observations of the S–L 9 fragment K to dust comae models will show that it was indeed an active, dust-producing comet. Estimates of its dust size distribution, mass loss rates, and dust outflow velocities are presented.

Correspondence to: T. W. Rettig

The activity of comet Shoemaker–Levy 9

Determining whether comet S–L 9 was active or dormant is necessary in order to successfully interpret the dust observations as well as to correctly infer the dusty-gas dynamical processes that may have occurred on its cometary surfaces. In fact, the distinction between activity versus dormancy alters the inferred mass of the S–L 9 dust grains by several orders of magnitude. According to the dormant-comet hypothesis, if most of the observed S–L 9 dust had been emitted by the comet fragments during the months just following the 1992 tidal breakup event and that S–L 9 had been relatively inactive ever since (e.g. Sekanina *et al.*, 1994; Sekanina, 1996a), then one must conclude that the surviving comae grains observed one to two years later were large, having sizes exceeding about 1 cm. Initially, much smaller grains may once have been present but they had since been swept from the fragments' comae by solar radiation pressure. However if the S–L 9 fragments were instead continuously emitting dust, then much smaller grains could have steadily replenished the comae as they continually drifted down the dust tails due to radiation pressure (e.g. Hahn *et al.*, 1996).

Regardless of whether the comet fragments were active or dormant, there could not have been a large contribution to the observed comae optical depth by grains much smaller than a few microns (e.g. Sekanina *et al.*, 1994; Hahn *et al.*, 1996; Sekanina, 1996a). This fact may be inferred from the observed dust tails' orientations. As cometary dust grains recede anti-sunward due to radiation pressure, keplerian shear causes the grains to drift in the direction opposite of the comet's velocity vector. In heliocentric

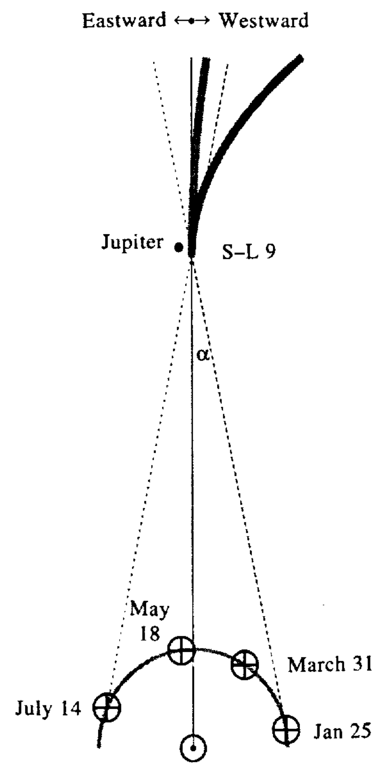

Fig. 1. Lines of sight from Earth ⊕ to S–L 9 are shown for selected HST observations acquired in 1994. A continuous stream of dust grains larger than about 5 μm contribute curved tails that always appear west of the fragment (dark grey curve), whereas smaller grains contribute straighter tails that appear east of the fragment (light grey curve) when observed after solar opposition. Dust tails are not drawn to scale

space, comet S L 9 was moving roughly eastward at approximately Jupiter's orbital velocity,[1] so keplerian shear was responsible for bending the dust tails west of the anti-solar direction. However the orientation of the tails projected onto an Earth-observer's sky plane depended upon the degree of the tail's curvature, and this was governed by the dust grains' size. Smaller grains that were rapidly accelerating anti-sunward gave rise to straighter tails, whereas large and slowly drifting grains contributed shorter tails having greater curvature. A schematic diagram of the Sun–comet–Earth viewing geometry for HST observations acquired in 1994 is sketched Fig. 1. This diagram indicates that the dust tails should always have appeared west of the fragments when viewed prior to solar opposition. But after solar opposition, if there were detectable quantities of grains smaller than a critical size, the dust tails would have rotated 180° from west to east on the sky plane. The critical grain size is about 5 μm for S–L 9 (Hahn *et al.*, 1996). It is important to realize that grains larger than this threshold would have contributed tails that would always have appeared west of the fragments when viewed either before or after solar opposition (see Fig. 1).

Comet S–L 9 was observed through two successive solar oppositions and no eastward dust features were detected (Sekanina *et al.*, 1994; Chernova *et al.*, 1996). Prior studies of S–L 9 often imply or conclude that the fragments were relatively dormant due to the absence of any eastward dust features (e.g. Sekanina *et al.*, 1994; Chernova *et al.*, 1996; Sekanina, 1996a). However this conclusion is premature since the observed dust tail orientations were consistent with both the active *and* the dormant comet hypotheses. The westward tail orientations observed after opposition instead provide an upper limit on the rate at which an S–L 9 fragment could have emitted grains smaller than a few microns, which is about 0.5 kg s^{-1} as estimated by Sekanina (1996a) based on HST detection limits.

Frequently, cometary dust emission occurs from a few discrete spots on the surface a comet nucleus which, if rotating, can produce dust streams and spirals sometimes seen propagating through a dust coma. It should be noted that comet S–L 9 exhibited rather featureless dust comae which have also been interpreted as an indicator of the fragment's *inactivity* (e.g. Sekanina, 1996a). However, a featureless dust coma is not a strict indicator of inactivity, for it is also consistent with dust emission that was more evenly distributed across a fragment's sunlit surface. This is a reasonable possibility considering the S L 9 fragments had effectively been stripped of any ancient surface mantle during the tidal disruption event which might otherwise have localized dust production to discrete spots.

There are, however, two lines of evidence that suggest S L 9 had been actively replenishing its dust comae. The first is that contour maps of the light distribution in the fragments' innermost $\approx 1''$ comae regions remained quite circular throughout most of the comet's orbit[2] (Weaver *et al.*, 1994, 1995; Hahn *et al.*, 1996; Rettig *et al.*, 1996b). It has been noted that if S–L 9 had been dormant and its comae had consisted of large grains simply co-orbiting with the fragments, then the inner comae contours should have become progressively elongated along the fragment train axis as the fragment train itself lengthen with time (Weaver *et al.*, 1995; Hahn *et al.*, 1996; Weissman, 1996). In contrast, a comet that continuously replenishes its dust comae will maintain circular isophotes in its inner coma, as was exhibited by S–L 9 throughout most of its orbit.

A second line of evidence that favors activity is the comae surface brightness profiles. An idealized comet experiencing steady and isotropic dust emission will develop a dust coma having a column density varying as ρ^{-1} with projected distance ρ from the coma photocenter. When the effects of radiation pressure acting upon a distribution of grains are considered, the brightness profile along the tail still varies as ρ^{-1} (generalizing the results of Wallace and Miller (1958)) whereas the azimuthally averaged brightness profile will develop a $\rho^{-3/2}$ power law for sufficiently large ρ (Jewitt and Meech, 1987). Brightness profiles for fragment K, given in Fig. 2, clearly evidence such phenomena. All of the bright, on-axis frag-

[1]Except just prior to impact, the velocity of S–L 9 relative to Jupiter was small compared to the orbital velocity of the Jupiter/S–L 9 system about the Sun. Jupiter's gravity did not play a significant role in determining the appearance of the S–L 9 comae and tails until about a month before impact (Hahn *et al.*, 1996).

[2]The exception, of course, occurred during the month just prior to impact as the comae and tails become progressively elongated along the comet–Jupiter direction.

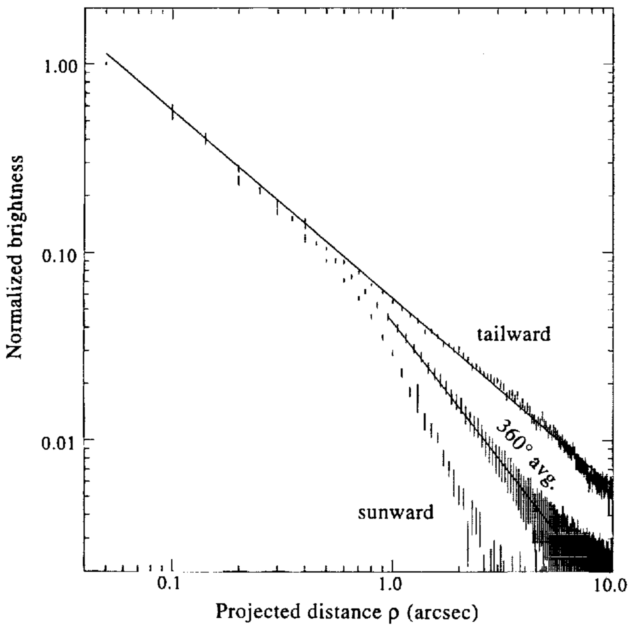

Fig. 2. Sunward, tailward, and azimuthally averaged (360°) surface brightness profiles of fragment K on March 30, 1994. A ρ^{-1} curve is drawn over the tailward profile and a $\rho^{-3/2}$ curve is plotted over the azimuthally averaged profile beyond $\rho > 1''$

ments imaged with HST throughout 1994 have comae light distributions similar[3] to Fig. 2 (Hahn *et al.*, 1996). It should be noted that brightness profiles extracted from the 1993 observations of S–L 9 differ distinctly from Fig. 2 and obey a $\approx\rho^{-0.7}$ dependence (from Fig. 6 of Jewitt (1995), see also Weaver *et al.* (1994)). This suggests that the S–L 9 dust production rate may have been decreasing with time prior to the 1994 observations considered here.

Spectroscopic searches for sublimating cometary gases have yielded null results for S–L 9 (Cochran *et al.*, 1994; Weaver *et al.*, 1994, 1995; Stüwe *et al.*, 1995), which is not regarded as unusual for small icy bodies 5.4 AU away from the Sun (Weissman, 1996). An unobserved surface gas flow is the most likely source of the observed dust emission, although alternate theories exist (see Olson and Mumma, 1994; Rettig *et al.*, 1996a). While only cursory comparisons of the appearance of dormant comet models to the observations have been made (Hahn *et al.*, 1996), their ability to fully explain the observed S–L 9 phenomena are not promising. Below we describe Monte Carlo simulations of an active comet in S–L 9's orbit about Jupiter. Synthetic images of model comae are constructed, and a search of parameter space provides excellent fits to the HST observations of fragment K. Fragment K's grain size and outflow velocity distributions are presented as well as its dust phase law coefficient and an upper limit on the fragment's radius.

Simulations of an S–L 9 coma and tail

Synthetic images of cometary dust comae and tails have been computed for comet S–L 9. By fitting model images to the sequence of S–L 9 observations obtained with the HST throughout 1994, and minimizing the fit's χ^2, the comet's grain size and outflow velocity distributions are extracted. Only a brief description of the modeling efforts is described here; a detailed account of shall be provided in a future communication as well as results obtained from observations of several other S–L 9 fragments.

The motion of a model S–L 9 fragment is numerically integrated forward in time following the moment of tidal breakup. As it orbits Jupiter, the simulated comet fragment ejects dust grains of various radii R at velocity $V(R)$ in random directions from its sunlit hemisphere. The model nucleus and its dust grains are subject to jovian and solar gravities with the grains also experiencing radiation pressure appropriate for their size. The model's dust size distribution is divided into nine discrete size bins ranging from $R = 1\ \mu$m on up to 1 cm. The allowed ejection velocities $V(R)$ are similarly discrete on $0.25\ \mathrm{m\,s^{-1}}$ velocity intervals (this quantization of the problem makes it computationally tractable). If $N(R,t)$ is defined as the cumulative number of all grains having radii smaller than R emitted by a given S–L 9 fragment up until some time t, then the task at hand is to solve for $\mathrm{d}\dot{N}(R,t) \approx \Delta R\, \mathrm{d}\dot{N}(R,t)/\mathrm{d}R$, which is the differential dust production rate of all grains in the size interval $R \pm \Delta R/2$ at time t. The velocity distribution $V(R)$ must also be solved for each size bin R. An important assumption made here is that the differential dust production rate $\mathrm{d}\dot{N}(R)$ is constant with time.[4] The comet dust is also assumed to obey the usual phase law $\log\psi(\alpha) = -\alpha\beta/2.5$, where α is the Sun–comet–Earth phase angle and the free parameter β is the phase coefficient. The additional light contributed by an unresolved spherical fragment of radius R_f is also included, and it is assumed to have a light distribution given by the HST point-spread-function. Thus 20 parameters specify a simulated set of S–L 9 observations—a $\mathrm{d}\dot{N}(R)$, $V(R)$ pair for each grain size bin plus β and R_f. Once a set of parameters are chosen, brightness maps of the coma and tail are computed for various observation dates.

The downhill simplex method is used to search the available parameter space and minimize the fit's χ^2 (Nelder and Mead, 1965; Press *et al.*, 1994). A time-sequence of contour maps of fragment K observed with HST is given in Fig. 3 as well as the resulting isophotes of the fitted synthetic image. Although discrepancies exist between the observed and modal isophotes at faint light levels, there is overall good agreement between the observations and the fit. Figure 4 shows the fragment's dust production distribution $\mathrm{d}\dot{N}(R)$ and its mass loss distribution $\mathrm{d}\dot{M}(R) = (4\pi/3)\rho_g R^3\, \mathrm{d}\dot{N}(R)$ which assumes a dust geometric albedo of 0.04 and a grain mass density $\rho_g = 1\ \mathrm{g\,cm^{-3}}$. The arrows represent upper limits on the production rates for the indicated size bins. These findings are typical of many comets in that production of the smallest grains are numerically favored but total mass loss rates are governed by the largest grains ejected. The mass

[3]Again the exception is just before impact when Jupiter's gravity altered the coma/tail structures. Also, several of the dim, off-axis fragments did not exhibit profiles like those seen in Fig. 2.

[4]The fragment's $\approx\rho^{-1}$ and $\approx\rho^{-3/2}$ brightness profiles, as well as its nearly constant distance from Sun, suggest (but do not guarantee) that its dust production rate did not vary significantly during the span of observations considered here.

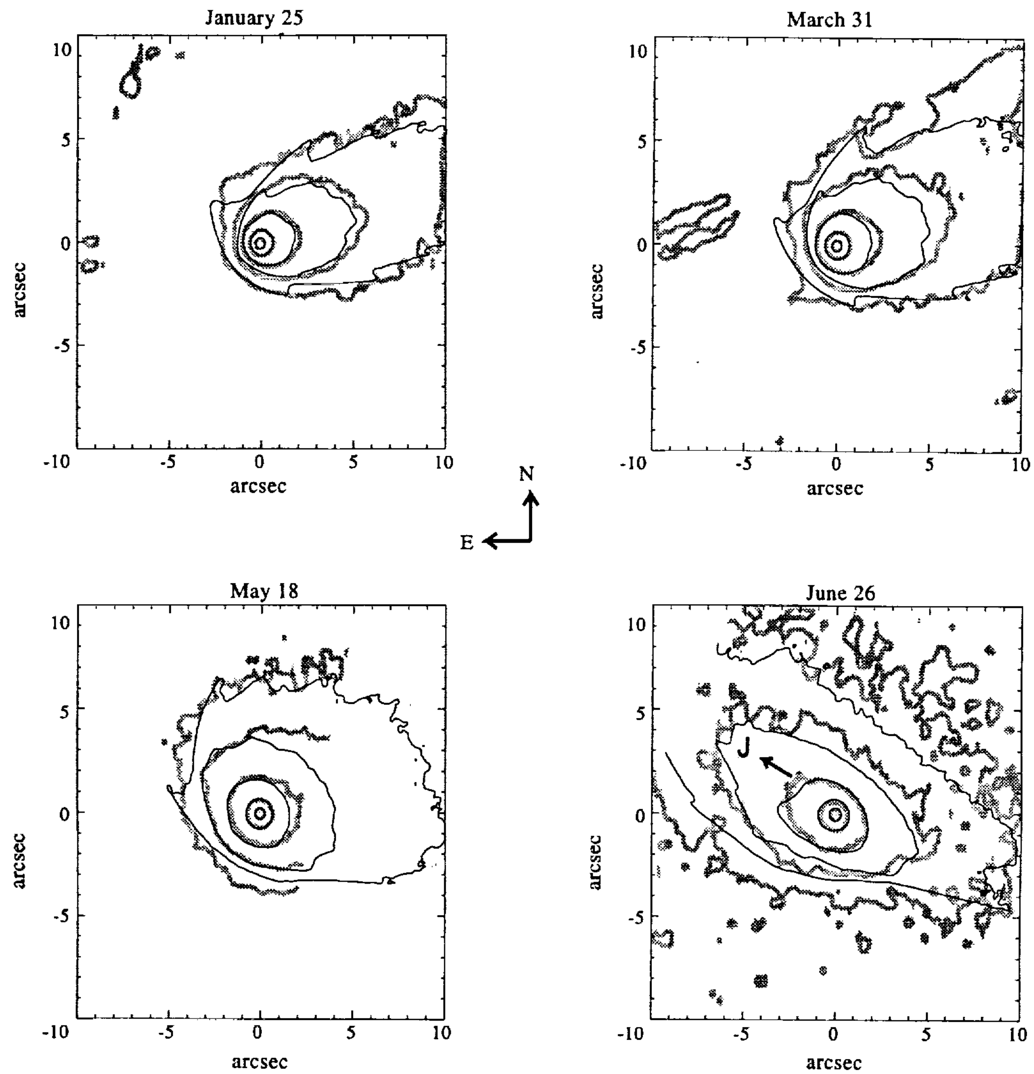

Fig. 3. Contour maps of fragments K (gray curves) and the fitted synthetic images (black curves). The coma observed on May 18 was clipped by the detector edge, and the "fins", along the faint isophotes are an artifact of the model which ejects dust having discrete, rather than continuous sizes and velocities. A star trail lies north of the fragment on March 31, and the arrow in the June 27 figure indicates the projected direction to Jupiter

loss rate of grains detected in fragment K's coma ($30\,\mu m \lesssim R \lesssim 3$ mm) is $\dot{M} \simeq 22 \pm 5\,kg\,s^{-1}$. Evidently, coma grains smaller than $30\,\mu m$ did not contribute a detectable amount of light scattering cross section, so only upper limits on their production rates are obtained. It is noted here that the mass loss rate for grains smaller than $3\,\mu m$ is at most $0.1\,kg\,s^{-1}$ and well below Sekanina's earlier upper limit.

It is interesting to compare the grain size distribution for fragment K with that for comet Halley. As is evident in Fig. 4, a single power law cannot accurately represent the fragment's grain size distribution. Nonetheless, computing the logarithm slope of $d\dot{N}(R)$ over the $30\,\mu m \lesssim R \lesssim 3$ mm size interval indicates $d\dot{N}(R) \propto R^{-a}$ with $a = 2.2 \pm 0.2$, which is considerably flatter than the $R^{-3.7}$ power law measured for comet Halley (Tokunaga *et al.*, 1986; Waniak, 1992). If comet S–L 9 had produced small grains in the same proportions as comet Halley, then they would have been well above detection limits, as indicated by Fig. 4.

The uncertainties quoted in Fig. 4 are 68% confidence intervals in the model parameters where $\rho_g = 1\,g\,cm^{-3}$ and $a = 0.04$ has been assumed. However our systematic uncertainties are affected by the unknown grain density and albedo. Radiation pressure sorts dust grains according to the product $\rho_g R$, so if the true S–L 9 grain density ρ_g differs from the value assumed here then the R axis in Figs 4 and 5 should be divided by a factor ρ_g expressed in cgs units. The observed flux reflected by each grain size bin determines $aR^2\,d\dot{N}(R)$, so if an alternate albedo a is also preferred, the grain production rates in Fig. 4 should be multiplied by $0.04\rho_g^2/a$. If ρ_g is independent of grain size (which might not be true if smaller cometary grains are fluffy instead of compact) then it can be shown that the mass loss rates $d\dot{M}(R) \propto \rho_g R^3\,d\dot{N}(R)$ are independent of the assumed grain density but still uncertain by a factor of $0.04/a$.

The dust outflow velocity distribution $V(R)$ for fragment K is given in Fig. 5 for the $30\,\mu m \leq R \leq 3$ mm grains, which, if described by a power law, would obey $V \propto R^{-b}$

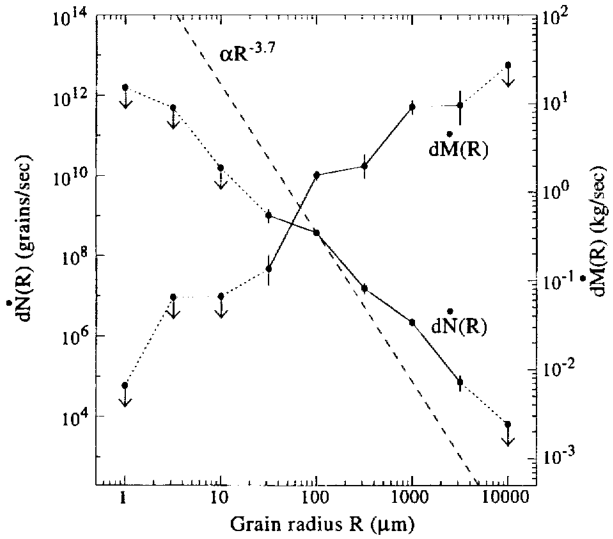

Fig. 4. Fragment K's differential dust production rate $d\dot{N}(R)$ and mass production rate $d\dot{M}(R)$ as a function of grain radius R. Arrows indicate upper limits. The dashed curve has the same logarithmic slope as an $R^{-3.7}$ Halley-type grain size distribution

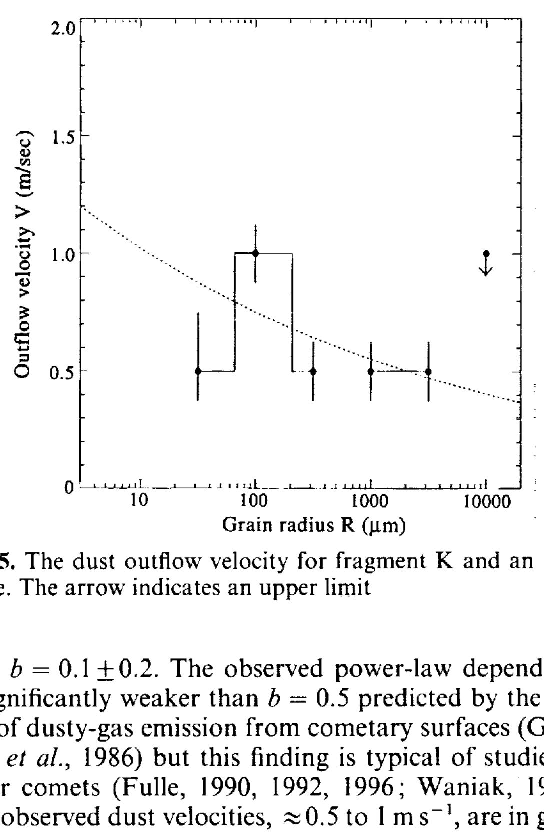

Fig. 5. The dust outflow velocity for fragment K and an $R^{-0.1}$ curve. The arrow indicates an upper limit

with $b = 0.1 \pm 0.2$. The observed power-law dependence is significantly weaker than $b = 0.5$ predicted by the theory of dusty-gas emission from cometary surfaces (Gombosi *et al.*, 1986) but this finding is typical of studies of other comets (Fulle, 1990, 1992, 1996; Waniak, 1992). The observed dust velocities, ≈ 0.5 to $1\ \mathrm{m\,s^{-1}}$, are in good agreement with earlier estimates (Hahn *et al.*, 1996; Rettig *et al.*, 1996b), but they are significantly slower than the outflow velocities measured for large grains emitted by other distant comets: $V \approx 15\ \mathrm{m\,s^{-1}}$ for Schwassmann–Wachmann 1 (S–W1) at 6 AU (Fulle, 1992), $V > 32\ \mathrm{m\,s^{-1}}$ for Hale–Bopp at 7 AU (Kidger *et al.*, 1996), $V \approx 5\ \mathrm{m\,s^{-1}}$ for Chiron at 9 AU (Fulle, 1994), and $V \approx 25\ \mathrm{m\,s^{-1}}$ for Halley at 14 AU (Sekanina *et al.*, 1992). The low velocities observed in S–L9 may indicate that its relatively large grains were poorly coupled to an unseen gas flow.

The parameter search algorithm yielded a phase law coefficient $\beta = 0.010 \pm 0.006$ magnitudes deg^{-1}. However the fitting algorithm could not uniquely disentangle any light reflected by an embedded comet fragment from that contributed by the surrounding dust coma. Only an upper limit of $R_f < 1.2$ km is obtained for fragment K's radius assuming an $a = 0.04$ albedo. This limit is about two times tighter than that reported by Weaver *et al.* (1995) and is slightly smaller than the size estimate given by Sekanina (1996b). Note that even smaller size limits/estimates have been obtained from models of the tidal disruption of the S–L9 progenitor [$R_f \approx \mathcal{O}(0.4)$ km (Asphaug and Benz, 1996)], models of the Jupiter impact events [$R_f \lesssim 0.5$ km (Mac-Low, 1996)], as well as the minimum impactor size that may be inferred from the amount of CO observed in Jupiter's atmosphere at the K impact site [$R_f \gtrsim \mathcal{O}(0.4)$ km (Lellouch, 1996)], the source of which is thought to be of cometary origin.

The lower limit on the fragment's radius is $R_{min} = (3\dot{M}\,\Delta t/4\pi\rho_f)^{1/3} \approx 0.4$ km in order for a fragment of density $\rho_f \approx 0.6\ \mathrm{g\,s^{-1}}$ to sustain a dust production rate of $\dot{M} \simeq 22\ \mathrm{kg\,s^{-1}}$ during the $\Delta t \simeq 2$ yr time interval between breakup and impact. Consequently if it had an initial size smaller than 0.4 km, it would have completely evaporated before striking Jupiter. However, fragment K was indeed observed to strike Jupiter. Supposing this fragment maintained a constant dust production rate during its final orbit, then with an initial fragment radius of at least 0.5 km, the final impactor radius would have had been 0.4 km or larger and would have ejected less than half its mass. Similarly, the smaller fragments F, J, P_1, P_2, T, and U did not exhibit any impact signatures (Hammel *et al.*, 1995; Chodas and Yeomans, 1996), so perhaps they simply exhausted most of their mass before they could strike the planet.

Conclusions

Since molecular fluorescence from any cometary gases were below detection limits, it is only from pre-impact observations of the dust that one might glean further insight into the structural properties of the tidally disrupted comet S–L9 fragments as well as the physics of their cometary atmospheres. For this reason it is critically important to correctly infer the history of dust emission by S–L9 and its grain sizes and outflow velocities. The photometry of S–L 9 favors an active-comet hypothesis over dormancy, as evidenced by the circular isophotes in its inner comae and its ρ^{-1} and $\rho^{-3/2}$ brightness profiles. Detailed comparisons of observations to an active-comet model further strengthens this contention.

The appearance of fragment K's coma and tail at visible wavelengths was governed by relatively large $30\ \mu m \lesssim R \lesssim 3$ mm grains ejected at velocities $V \simeq 0.5$–$1.0\ \mathrm{m\,s^{-1}}$. Grains 10 μm and smaller were not detected above a one-σ confidence level, but it is reasonable to assume they were produced at a rate below the $\approx 0.1\ \mathrm{kg\,s^{-1}}$ detection limit. The non-detection of small grains that are otherwise characteristic of most other comets is due to S–L 9's rather flat size distribution, $d\dot{N}(R) \propto R^{-2.2 \pm 0.2}$. One may speculate that its unusual size distribution was a consequence of the comet's tidally disrupted nature. Dust grains from most comets emanate from, and are perhaps filtered by, an ancient overlying surface mantle. However a surface mantle is absent on a tidally disrupted comet, and this may have permitted the large S–L 9 dust grains to escape with greater ease and result in a dust size distribution that was flatter than seen in most comets. The large grains seen in the S–L 9 comae may also be an indicator of the particular ice species that was responsible for the comet's dust emission. At S–L 9's distance from the Sun, water production would have been too feeble to launch any grains larger than $\approx \mathcal{O}(1)\,\mu$m from the surface of an $R_f \approx \mathcal{O}(1)$ km comet fragment (see Hahn *et al.*, 1996). However models indicate that the sublimation of more volatile species such as CO or CO_2 may have been sufficiently vigorous to loft grains as large as a few millimeters.

During the 1994 observations, fragment K was ejecting the $30\,\mu\text{m} \lesssim R \lesssim 3$ mm grains at a rate of $\dot{M} = 22 \pm 5\,\text{kg s}^{-1}$. In order to sustain this rather vigorous mass loss rate the radius of fragment K must have been $R_f > 0.4$ km at the time of breakup, while the dust coma modeling indicates that $R_f < 1.2$ km during the 1994 observations. Thus without ever observing fragment K directly, its radius is constrained to lie within a fairly narrow size interval.

A comparison of dust production by the S–L 9 fragment K to comets S–W 1 and Chiron is in order; these bodies have estimated mass loss rates of ≈ 600 and $\approx 2\,\text{kg s}^{-1}$, respectively (Fulle, 1992, 1994). However these comets are much larger than S–L 9, having radii $R_{\text{S–W 1}} \approx 15$ km (Meech *et al.*, 1993) and $R_{\text{Chiron}} \approx 84$ km (Altenhoff and Stumpff, 1995). A comparison of mass loss rates *per nucleus surface area* reveals that the surface of fragment K was at least ≈ 6 times more active than S–W 1, and at least $\approx 5 \times 10^3$ times greater than Chiron. Thus this S–L 9 fragment, and perhaps all the others, were *extremely* active in comparison to other comets orbiting at comparable distances from the Sun. This fact may also be a consequence of S–L 9's tidal disruption which stripped any surface mantle from the fragments that might otherwise have constricted their dust production.

Acknowledgements. This research was performed while J.M.H. was in residence at the University of Notre Dame. Support for this work was also provided by NASA through grant 5624.21-93A from the Space Telescope Science Institute which is operated by the Association of Universities for Research in Astronomy, Incorporated, under NASA contract NAS5-26555. This paper represents contribution 924 from the Lunar and Planetary Institute, operated by the Universities Space Research Association NASA contract NA6W 4575.

References

Altenhoff, W. J. and Stumpff, P. (1995) Size estimate of "asteroid" 2060 chiron from 250 GHz measurements. *Astron. Astrophys.* **293,** L41–L42.

Asphaug, E. and Benz, W. (1996) Size, density, and structure of Comet Shoemaker–Levy 9 inferred from the physics of tidal breakup. *Icarus* **121,** 225–248.

Chernova, G. P., Jockers, K. and Kiselev, N. N. (1996) Imaging photometry and color of Comet Shoemaker–Levy 9. *Icarus* **121,** 38–45.

Chodas, P. W. and Yeomans, D. K. (1996) The orbital motion and impact circumstances of Comet Shoemaker–Levy 9. In *The Collision of Comet Shoemaker–Levy 9 and Jupiter*, eds K. Noll, H. A. Weaver and P. D. Feldman, pp. 1–30. Cambridge University Press, Cambridge.

Cochran, A. L., Whipple, A. L., MacQueen, P. J., Shelus, P. J., Whited, R. W. and Claver, C. F. (1994) Preimpact characterization of P/Comet Shoemaker–Levy 9. *Icarus* **112,** 528–532.

Fulle, M. (1990) Meteoroids from short period comets. *Astron. Astrophys.* **230,** 220–226.

Fulle, M. (1992) Dust from short period comet P/Schwassmann–Wachmann 1 and replenishment of the interplanetary dust cloud. *Nature* **359,** 42–44.

Fulle, M. (1994) Spin axis orientation of 2060 Chiron from dust coma modeling. *Astron. Astrophys.* **282,** 980–988.

Fulle, M. (1996) Dust environment and nucleus spin axis of comet P/Temple 2 from models of the infrared dust tail observed by IRAS. *Astron. Astrophys.* **311,** 333–339.

Gombosi, T. I., Nagy, A. F. and Cravens, T. E. (1986) Dust and neutral gas modeling of the inner atmospheres of comets. *Rev. Geophys.* **24,** 667–700.

Hahn, J. M., Rettig, T. W. and Mumma, M. J. (1996) Comet Shoemaker–Levy 9 dust. *Icarus* **12,** 291–304.

Hammel, H. B., Beebe, R. F., Ingersoll, A. P., Orton, G. S., Mills, J. R., Simon, A. A., Chodas, P., Clarke, J. T., De Jong, E., Dowling, T. E., Harrington, J., Huber, L. F., Karkoschka, E., Santori, C. M., Toigo, A., Yeomans, D. and West, R. A. (1995) HST imaging of atmospheric phenomena created by the impact of Comet Shoemaker–Levy 9. *Science* **267,** 1288–1296.

Jewitt, D. (1995) Pre-impact observations of Comet Shoemaker–Levy 9. In *Proc. European SL-9/Jupiter Workshop*, eds R. West and H. Böhnhardt, ESO Conference and Workshop Proceedings No. 52, pp. 1–4.

Jewitt, D. C. and Meech, K. J. (1987) Surface brightness profiles of 10 comets. *Astrophys. J.* **317,** 992–1001.

Kidger, M. R., Serra-Ricart, M., Bellot-Rubio, L. R. and Casas, R. (1996) Evolution of a spiral jet in the inner coma of Comet Hale–Bopp (1995 O1). *Astrophys. J.* **461,** L119–L122.

Lellouch, L. (1996) Chemistry induced by impacts: observations. In *The Collision of Comet Shoemaker–Levy 9 and Jupiter*, eds K. S. Noll, H. A. Weaver and P. D. Feldman, pp. 213–242. Cambridge University Press, Cambridge.

Mac-Low, M.-M. (1996) Entry, and fireball models vs. observations: what have we learned? In *The Collision of Comet Shoemaker–Levy 9 and Jupiter*, eds K. S. Noll, H. A. Weaver and P. D. Feldman, pp. 157–182. Cambridge University Press, Cambridge.

Meech, K. J., Belton, M. J. S., Mueller, B. E. A., Dicksion, M. W. and Li, H. R. (1993) Nucleus properties of P/Schwassmann–Wachmann 1. *Astronom. J.* **106,** 1222–1236.

Nelder, J. A. and Mead, R. (1965) A simplex method for function minimization. *Comput. J.* **7,** 308–313.

Olson, K. M. and Mumma, M. J. (1994) Simulations of the breakup and dynamical evolution of Comet Shoemaker/Levy 9 employing a swarm model. *Bull. Am. Astron. Soc.* **26,** 1574–1575.

Press, W. H., Flannery, B. B., Teukolsky, S. A. and Vettarling, W. T. (1994) *Numerical Recipes in C.* Cambridge University Press, Cambridge.

Rettig, T. W., Mumma, M. J., Sobczak, G. J., Hahn, J. M. and DiSanti, M. (1996a) The nature of Comet Shoemaker–Levy 9 sub-nuclei from analysis of pre-impact HST images. *J. Geophys. Res. Planets* **101,** 9271–9282.

Rettig, T. W., Sobczak, G. W. and Hahn, J. M. (1996b) Dust outflow velocity for Comet Shoemaker–Levy 9. *Icarus* **121,** 281–290.

Sekanina, Z. (1996a) Tidal breakup of the nucleus of Comet Shoemaker Levy 9. In *The Collision of Comet Shoemaker Levy 9 and Jupiter*, eds K. S. Noll, H. A. Weaver and P. D. Feldman, pp. 55–80. Cambridge University Press, Cambridge.

Sekanina, Z. (1996b) Fragmentation of Comet Shoemaker–Levy

9's nuclei during flight through the jovian atmosphere. In *Physics, Chemistry, and Dynamics of Interplanetary Dust*, eds B. A. S. Gustafson and M. S. Hanner, pp. 383–386.

Sekanina, Z., Larson, S. M., Hainaut, O., Smette, A. and West, R. M. (1992) Major outburst of periodic comet Halley at a heliocentric distance of 14 AU. *Astron. Astrophys.* **263,** 367–386.

Sekanina, Z., Chodas, P. W. and Yeomans, D. K. (1994) Tidal disruption and the appearance of periodic comet Shoemaker Levy 9. *Astron. Astrophys.* **289,** 607–636.

Stüwe, J. A., Schulz, R. and A'Hearn, M. F. (1995) NTT observations of Shoemaker–Levy 9. In *Proc. Europoean SL-9/ Jupiter Workshop*, eds R. West and H. Böhnhardt, ESO Conference and Workshop Proceedings No. 52, pp. 17–22.

Tokunaga, A. T., Golisch, W. F., Griep, D. M., Kaminski, C. D. and Hanner, M. S. (1986) The NASA Infrared Telescope Facility Comet Halley monitoring program—I. Preperihelion results. *Astronom. J.* **92,** 1183–1190.

Wallace, L. V. and Miller, F. D. (1958) Isophote configurations for model comets. *Astronom. J.* **63,** 213–219.

Waniak, W. (1992) A Monte Carlo approach to the analysis of the dust tail of comet P/Halley. *Icarus* **100,** 154–161.

Weaver, H. A., Feldman, P. D., A'Hearn, M. F., Arpigny, C., Brown, R. A., Helin, E. F., Levy, D. H., Marsden, B. G., Meech, K. J., Larson, S. M., Noll, K. S., Scotti, J. V., Sekanina, Z., Shoemaker, C. S., Shoemaker, E. M., Smith, T. E., Storrs, A. D., Yeomans, D. K. and Zellner, B. (1994) Hubble Space Telescope observations of Comet P/Shoemaker–Levy 9 (1993e). *Science* **263,** 787–791.

Weaver, H. A., A'Hearn, M. F. A., Arpigny, C., Boice, D. C., Feldman, P. D., Larson, S. M., Larny, P., Levy, D. H., Marsden, B. G., Meech, K. J., Noll, K. S., Scotti, J. V., Sekanina, Z., Shoemaker, C. S., Shoemaker, E. M., Smith, T. E., Stern, S. A., Storrs, A. D., Trauger, J. T., Yeomans, D. K. and Zellner, B. (1995) Hubble Space Telescope (HST) observing campaign on Comet Shoemaker–Levy 9. *Science* **267,** 1282–1287.

Weissman, P. R. (1996) If it quacks like a comet.... *Icarus* **121,** 275–280.